RSC Advances

PAPER

View Article Online
View Journal | View Issue

Cite this: *RSC Adv.*, 2026, **16**, 19542

Programmable antimicrobial graphene oxide-silver nanoparticle-poly(acrylic acid) hydrogels for smart regenerative medicine

Anika Tabassum Promi,†[ab] Md. Kaium Hossain,†[c] Shaikat Chandra Dey,[ad] Aanshi Tiwari,[e] Nusrat Mustary,[f] Md. Mizanur Rahaman,[g] Otun Saha,[h] Ayushi Tiwari,[e] Yogesh Shukla,[e] Ashutosh Tiwari[e] and Md. Ashaduzzaman *[ae]

Hydrogels with tunable physicochemical properties are being increasingly explored for advanced biomedical applications. In this study, two composite hydrogels were rapidly fabricated through the free radical polymerization of acrylic acid (AA) with the *in situ* formation of silver nanoparticles (AgNPs) in the presence and absence of graphene oxide (GO). The resulting GO-AgNP-poly(acrylic acid) and AgNP-poly(acrylic acid) hydrogels have been systematically characterized by functional group analysis, crystallinity, thermal stability, elemental analysis, and morphological studies using attenuated total reflectance-infrared spectroscopy, X-ray diffraction, thermogravimetric analysis, energy dispersive spectroscopy, and field-effect scanning electronic microscopy, respectively. Both hydrogels demonstrated pH-switchable swelling–deswelling (on/off) behavior; however, the incorporation of GO provided interfacial channels that enhanced solvent interaction. The *in situ*-formed AgNPs (~13 nm) endowed the hydrogels with strong antibacterial and *anti*-biofilm activity against both Gram-positive and Gram-negative bacterial strains. Cytotoxicity studies confirmed excellent biocompatibility with Vero, HeLa, and BHK-21 cell lines. The synergistic combination of pH-responsiveness, broad-spectrum antimicrobial activity, and cytocompatibility positions these novel composite hydrogels as promising candidates for smart wound healing and tissue engineering applications.

Received 6th December 2025
Accepted 8th March 2026

DOI: 10.1039/d5ra09443g

rsc.li/rsc-advances

1. Introduction

Hydrogels are a unique class of polymeric materials that have garnered considerable attention in recent decades due to their versatile physicochemical properties and broad applicability across various biomedical, pharmaceutical, environmental, and industrial domains. Hydrogels are three-dimensional, cross-linked networks of natural or synthetic polymers that can absorb and retain large quantities of water or biological fluids without undergoing dissolution.[1,2] The remarkable water-retention capacity arises from the hydrophilic functional groups within the polymer chains, and the structural stability is ensured through physical or chemical cross-linking. These materials combine solid-like mechanical integrity with liquid-like diffusion characteristics, enabling them to function as biomimetic scaffolds[3,4] and controlled-release matrices.

Hydrogels have undergone significant evolution since the pioneering development of poly(2-hydroxyethyl methacrylate) hydrogels in the 1960s, initially introduced for soft contact lenses.[5] The research was then expanded to explore diverse hydrogel formulations for applications including wound dressings, drug delivery, gene therapy, tissue engineering, bacterial infection prevention, biosensors, food packaging, edible films, agriculture, and water purification.[6–12] However, the biomedical sector has been particularly influential in driving innovation, as hydrogels offer crucial advantages, including biocompatibility, permeability to oxygen and nutrients, and the ability to mimic the properties of the extracellular matrix (ECM).

The compatibility of hydrogels with biological tissues makes them especially promising for wound healing, tissue engineering scaffolds, and drug delivery vehicles. In wound care, for example, hydrogels maintain a moist environment that accelerates epithelialization, protect against mechanical trauma,

[a]*Department of Applied Chemistry and Chemical Engineering, University of Dhaka, Dhaka 1000, Bangladesh. E-mail: azaman01@du.ac.bd; Tel: (+880) 1680–773–734*
[b]*Department of Chemistry, Virginia Tech, Blacksburg, USA*
[c]*Department of Chemistry, Bangladesh University of Engineering and Technology, Dhaka 1000, Bangladesh*
[d]*Department of Forest Biomaterials, North Carolina State University, Campus Box 8005, Raleigh, NC 27695, USA*
[e]*Institute of Advanced Materials, IAAM, Gammalkilsvägen 18, Ulrika 590 53, Sweden*
[f]*Department of Community Medicine, Dhaka National Medical College, 53/1 Johnson Road, Dhaka 1100, Bangladesh*
[g]*Department of Microbiology, University of Dhaka, Dhaka 1000, Bangladesh*
[h]*Department of Microbiology, Noakhali Science and Technology University, Noakhali 3814, Bangladesh*
† Anika Tabassum Promi and Md. Kaium Hossain have contributed equally.

absorb exudates, and deliver bioactive molecules such as antimicrobials, growth factors, or anti-inflammatory agents.[13,14] Furthermore, their high water content provides a soothing and cooling effect, making hydrogel dressings particularly useful for burns and painful wounds.[15]

Traditional hydrogel dressings, however, often face limitations, such as poor mechanical strength, limited responsiveness to the dynamic wound environment, and susceptibility to microbial contamination. These drawbacks have motivated the development of smart hydrogels, which are designed to respond to external stimuli such as pH, temperature, ionic strength, light, or redox conditions.[16] pH-responsive hydrogels are especially valuable in wound healing, as the pH of the wound microenvironment can fluctuate significantly during different stages of healing or in response to infection.[17] For example, acute wounds typically exhibit a slightly acidic pH (5.5–6.5), which is favorable for epithelialization, whereas chronic wounds often become alkaline (pH 7–9), which correlates with infection and delayed healing.[18] Smart hydrogels capable of swelling or shrinking in response to pH thus offer opportunities for controlled exudate absorption, site-specific drug release, and infection monitoring.

Among the synthetic hydrogel systems, poly(acrylic acid) (PAA)-based hydrogels have attracted considerable attention due to their outstanding water absorbency, biocompatibility, and tunable properties. PAA contains abundant carboxyl groups, which ionize in aqueous environments to produce electrostatic repulsion between polymer chains, resulting in dramatic swelling behavior.[19] This pH-dependent ionization makes PAA hydrogels particularly suitable for stimuli-responsive applications, including drug delivery and wound management.[20] PAA-based hydrogels are widely used as superabsorbent polymers in hygiene products, separation membranes, ion-exchange resins, and biomedical devices.[21] Their eco-friendly nature and ease of recovery from aqueous systems further enhance their attractiveness for sustainable applications. However, pristine PAA hydrogels suffer from limitations, including poor mechanical strength, low elasticity, and limited antimicrobial activity, which restrict their use in biomedical applications that require robustness and biofunctionality.[22] These drawbacks can be addressed by incorporating nanofillers or functional nanoparticles into the hydrogel matrix to create nanocomposite hydrogels with enhanced properties.

The incorporation of nanomaterials into hydrogels has emerged as a powerful strategy to improve their mechanical, physicochemical, and biological properties. Nanomaterials can serve as reinforcing agents, cross-linkers, or functional additives that impart novel features such as electrical conductivity, bioactivity, and antimicrobial behavior.[23] In particular, GO and AgNPs have garnered significant attention due to their synergistic potential in hydrogel systems. GO, a chemically oxidized form of graphene, consists of a single-layer carbon sheet decorated with oxygenated functional groups such as hydroxyl, epoxide, and carboxyl groups.[24] These functionalities make GO highly dispersible in aqueous media and chemically reactive, enabling strong interactions with polymer matrices. GO possesses a high surface area, excellent mechanical strength, and tunable electronic properties, which can reinforce hydrogel networks and improve their stability.[25] Furthermore, GO has been shown to exhibit antibacterial properties, attributed to mechanisms such as physical disruption of bacterial membranes by sharp nanosheets, oxidative stress induction, and extraction of phospholipids.[26,27]

The integration of GO into hydrogels has been reported to enhance swelling dynamics, mechanical performance, and antibacterial efficacy, making GO-polymer hydrogels promising candidates for biomedical applications.[28] For instance, GO-PAA composites demonstrate higher swelling ratios and improved structural integrity compared to pristine PAA hydrogels.[29] AgNPs are among the most widely studied antimicrobial nanomaterials. Their efficacy spans Gram-positive and Gram-negative bacteria, fungi, and even some viruses.[30] The antibacterial activity of AgNPs arises from multiple mechanisms: (i) the release of Ag^+ ions that interact with thiol groups in proteins, disrupting enzymatic activity; (ii) generation of reactive oxygen species (ROS) that induce oxidative stress, and (iii) direct damage to bacterial membranes and DNA.[31] Unlike conventional antibiotics, AgNPs act through multiple pathways, reducing the likelihood of resistance development.[32]

AgNPs embedded in hydrogel matrices act as sustained-release reservoirs, providing long-term antimicrobial protection at the wound site.[33] Several studies have demonstrated the efficacy of AgNPs-containing hydrogels as wound dressings, where they not only prevent infection but also promote faster wound closure and tissue regeneration.[34] Although GO and AgNPs individually enhance hydrogel performance, their synergistic incorporation into a PAA matrix offers unique advantages. GO provides mechanical reinforcement and additional antibacterial activity, while AgNPs deliver potent bactericidal effects. The functional groups on GO sheets can act as nucleation sites for *in situ* AgNP formation, ensuring uniform nanoparticle dispersion and stability within the hydrogel. This synergy has been shown to improve swelling, mechanical strength, and antibacterial activity while maintaining cytocompatibility.[35] Moreover, GO can act as a channel-forming agent, creating interfacial pathways within the hydrogel network that facilitate solvent penetration and swelling–deswelling dynamics.[36] This feature is particularly beneficial for pH-responsive hydrogels, where rapid on–off switching is desirable for smart biomedical applications.

Wound healing is a complex biological process involving inflammation, proliferation, and remodeling. Infection and biofilm formation are significant obstacles that can delay healing and lead to chronic wounds. Conventional wound dressings, such as gauze and cotton, often fail to prevent microbial colonization or provide an optimal healing environment.[37] Furthermore, chronic wounds often exhibit an alkaline pH, excessive exudation, and recurrent infections, necessitating advanced wound management strategies.[38] Smart hydrogels that combine pH responsiveness, antimicrobial activity, and cytocompatibility are ideally suited to address these challenges. Their ability to dynamically respond to changes in the wound microenvironment enables controlled fluid absorption, drug delivery, and infection

prevention. By incorporating both GO and AgNPs, hydrogels can simultaneously provide structural robustness, on–off swelling behavior, and broad-spectrum antimicrobial activity. Importantly, cytotoxicity studies have demonstrated that well-designed GO-AgNP-hydrogels are biocompatible with mammalian cells, making them safe for clinical applications.[39]

Building on this background, we report herein the fabrication of novel GO-AgNP-PAA and AgNP-PAA hydrogels *via* a rapid, surfactant- and cross-linker-free free radical polymerization of acrylic acid. The use of a simple, cost-effective, and scalable synthesis method differentiates this study from many earlier approaches that required additional reducing agents or stabilizers. The hydrogels were systematically characterized using ATR-IR, XRD, TGA, EDS, and FESEM to confirm their structural, thermal, and morphological features. The study further investigated their pH-responsive swelling behavior, antimicrobial activity against Gram-positive and Gram-negative bacteria, and cytocompatibility with mammalian cell lines (Vero, HeLa, BHK-21). The results demonstrate remarkable on–off swelling–deswelling switching, broad-spectrum antibacterial efficacy, and excellent biocompatibility, highlighting the hydrogels' potential for smart wound healing applications. This work, therefore, contributes to the growing field of multifunctional nanocomposite hydrogels, offering a platform that combines stimuli-responsive swelling, antimicrobial activity, and cytocompatibility through an environmentally friendly and scalable synthesis route. The findings may pave the way for clinical translation of next-generation wound-healing materials and provide insights for extending the approach to drug delivery, tissue engineering, and infection-resistant biomaterials.

2. Experimental

2.1. Materials

All chemicals used in this study were of analytical grade and employed without further purification unless otherwise specified. Acrylic acid (AA, 99%) and silver nitrate ($AgNO_3$) were purchased from Loba Chemie Pvt. Ltd Graphite powder and potassium persulfate were obtained from local suppliers. Sodium nitrate ($NaNO_3$), concentrated sulfuric acid (H_2SO_4, 98%), potassium permanganate ($KMnO_4$), and hydrogen peroxide solution (H_2O_2, 30%) were supplied by Sigma-Aldrich. Distilled water was used as the solvent in all experiments.

Acrylic acid served as the monomer for hydrogel formation due to its well-known hydrophilicity and pH-responsive properties, while potassium persulfate functioned as a thermal initiator. Silver nitrate was chosen as the precursor for the *in situ* synthesis of AgNPs, imparting antimicrobial properties to the hydrogel. Graphite powder was used as the starting material for the preparation of GO *via* a modified Hummers' method. The inclusion of GO was expected to enhance structural integrity and solvent-interaction channels, performing synergistically with the AgNPs.

2.2. Synthesis of graphene oxide

GO was synthesized using a modified Hummers' method, which is widely regarded as one of the most reliable procedures for producing GO with abundant oxygenated functional groups. These functionalities play a critical role in facilitating dispersion in aqueous solutions and providing nucleation sites for silver nanoparticle growth.

In a typical synthesis, 5.0 g of graphite powder and 2.5 g of $NaNO_3$ were slowly added to 115 mL of concentrated H_2SO_4 in an ice bath, ensuring vigorous stirring. The use of an ice bath at this stage was essential to control exothermic heat generation during the oxidation process. Subsequently, 15.0 g of $KMnO_4$ was gradually introduced while maintaining the reaction temperature below 44 °C to avoid violent oxidation. The mixture was stirred for 4 h, allowing for controlled intercalation of oxidizing agents into the graphite lattice.

An additional 85 mL of concentrated H_2SO_4 was added to strengthen the acidic environment, followed by dilution with 230 mL of distilled water. The suspension was then heated to 98 °C and stirred for 30 min to facilitate oxidation and exfoliation. A further 700 mL of distilled water was added, and stirring was continued for another 30 min. After cooling to room temperature, 30 mL of 30 wt% H_2O_2 was introduced to terminate the reaction, reducing residual manganese species and producing a bright yellow solution indicative of GO formation.

The suspension was allowed to settle overnight to enable the separation of layers. The resulting material was repeatedly washed with ~3 L of distilled water until a neutral pH was achieved, ensuring the removal of acid residues and salts. The final GO product was obtained by drying the precipitate at 60 °C for 24 h. The modified Hummers' method was selected because it generates GO sheets rich in hydroxyl, carboxyl, and epoxy groups, improving water dispersibility and providing interfacial bonding with the hydrogel matrix.

2.3. Synthesis of GO-AgNP-PAA hydrogel

The nanocomposite hydrogel was synthesized by the *in situ* free radical polymerization of acrylic acid in the presence of silver nitrate and GO (Fig. 1). This strategy was chosen to simultaneously form the polymeric hydrogel network and uniformly embed AgNPs and GO within the structure, thus ensuring intimate interaction among all components.

First, 1.0 g of $AgNO_3$ was dissolved in 20 mL of distilled water under continuous stirring. To this, 50 mg of as-prepared GO and 5 mL of acrylic acid were added. The mixture was subjected to sonication for 20 min to ensure complete exfoliation and homogeneous dispersion of GO nanosheets within the solution. The uniform distribution of GO was critical to ensure consistent mechanical reinforcement and the creation of interfacial solvent channels throughout the hydrogel.

Potassium persulfate (10 mg) was then introduced as a thermal initiator to trigger free-radical polymerization of acrylic acid. The mixture was stirred thoroughly and subsequently transferred to an oven maintained at 80 °C for 30 min. During this process, polymerization of AA resulted in the formation of a cross-linked hydrogel matrix, while $AgNO_3$ was reduced *in situ* to form AgNPs that were simultaneously immobilized within the matrix. The presence of GO provided nucleation sites for AgNPs formation, preventing aggregation

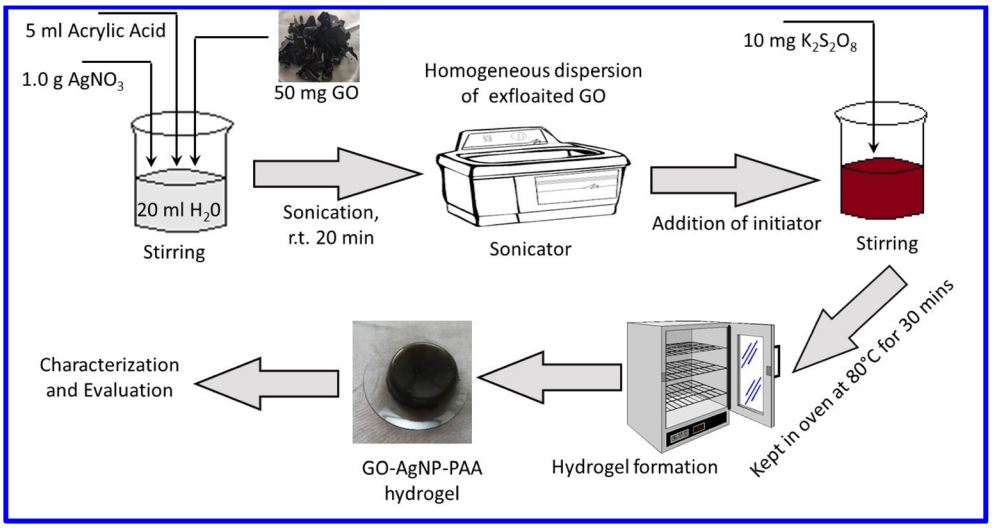

Fig. 1 Synthetic route for the hydrogel preparation using $AgNO_3$, GO and acrylic acid in the presence of a $K_2S_2O_8$ thermal initiator.

and ensuring uniform distribution of nanoparticles. The resulting product was a GO-AgNP-PAA hydrogel with enhanced structural and functional properties.

2.4. Synthesis of AgNP-PAA hydrogel

To evaluate the role of GO in modifying hydrogel performance, a control hydrogel (AgNP-PAA) was synthesized under identical conditions but without GO. For this, 1.0 g of $AgNO_3$ and 5 mL of acrylic acid were dissolved in 20 mL of distilled water. Potassium persulfate (10 mg) was added to initiate free radical polymerization, and the mixture was heated at 80 °C for 30 min to form the hydrogel. This control sample enabled the direct comparison of swelling, antimicrobial, and cytotoxicity properties, highlighting the specific contribution of GO incorporation.

2.5. Characterization of hydrogels

A combination of spectroscopic, diffraction, thermal, and microscopic techniques was employed to thoroughly characterize the hydrogels. Attenuated Total Reflectance Infrared (ATR-IR) spectra of GO, AgNP-PAA, and GO-AgNP-PAA hydrogels were recorded on a Shimadzu IRPrestige-21 spectrophotometer in the range 4000–400 cm^{-1}. This analysis provided information on functional groups and interactions between polymer chains, GO sheets, and AgNPs. Structural analysis was conducted using a Rigaku Ultima IV diffractometer with Cu Kα radiation ($\lambda = 1.5406$ Å) at 40 kV and 40 mA. Data were collected over a 2θ range of 10–80° at a scan rate of 3° min^{-1}. XRD patterns confirmed the crystallinity of embedded AgNPs and the structural arrangement of GO within the polymeric network. Thermal stability was assessed using a Shimadzu TGA-50 analyzer under a nitrogen atmosphere. Samples (4–8 mg) were heated from 25 °C to 800 °C at a rate of 10 °C min^{-1}. This analysis helped in understanding the degradation profile of the hydrogel, as well as the stabilizing effect of GO. Morphological features were investigated using scanning electron microscopy (JEOL JSM-6490LA, Tokyo, Japan) and field emission scanning electron microscopy (FESEM, JEOL JSM-7600F). Images were obtained at magnifications ranging from 500× to 1 000 00× at accelerating voltages of 5–20 kV. Energy dispersive X-ray spectroscopy (EDS) was employed to confirm the elemental composition and presence of Ag within the hydrogel. GO incorporation was expected to produce layered structures and solvent channels, which were examined *via* FESEM. The combined characterization ensured that the structural, thermal, and functional properties of the hydrogels were well documented and linked to their intended biomedical applications.

2.6. Antimicrobial activity

The antimicrobial properties of the hydrogels were evaluated using both Gram-positive and Gram-negative bacterial strains. Gram-negative strains included *Klebsiella* spp. (KH15), *Escherichia coli* (EH9), and *Pseudomonas* spp. (PsI1), while Gram-positive strains included *Staphylococcus aureus* (6 s). Additionally, *E. coli* DH5α was used as a reference strain.

The antibacterial activity was tested using the agar well diffusion method as described by Bauer *et al.*[40] Hydrogel samples were dispersed in distilled water at three different concentrations (10, 20, and 30 mg mL^{-1}) by sonication for 10–30 min to ensure uniform suspension. Wells were loaded with hydrogel dispersions, and plates were incubated under appropriate conditions. The diameters of the zones of inhibition were measured to assess antibacterial efficacy.

This step was critical for establishing the biomedical relevance of the materials. For wound healing applications, the prevention of microbial colonization and biofilm formation is essential to accelerate tissue regeneration and avoid chronic infection. Comparing GO-AgNP-PAA with AgNP-PAA allowed us to determine whether GO contributed synergistically to antimicrobial behavior. All antibacterial experiments were performed in triplicate, and inhibition zone diameters are presented as mean ± SD. Statistical significance among different hydrogel treatments and concentrations was analyzed using one-way ANOVA followed by Tukey's post hoc test, with $p < 0.05$ considered statistically significant.

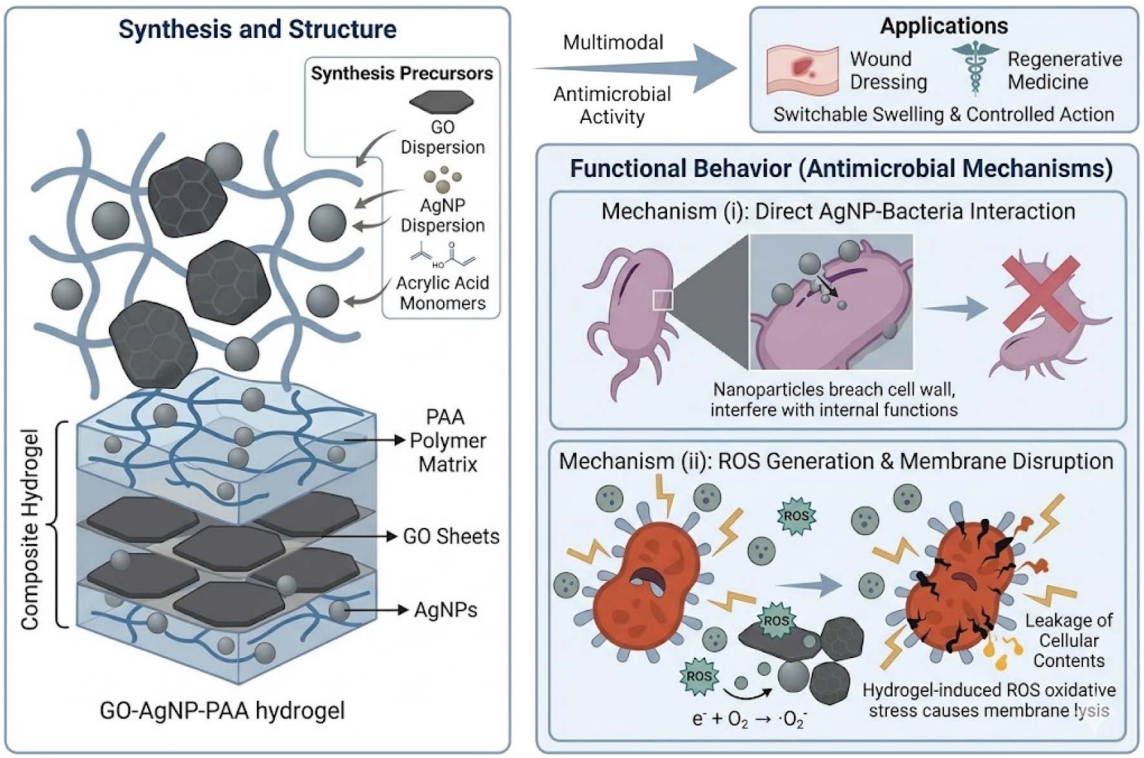

Fig. 2 Schematic of the synthesis and functional behavior of the GO-AgNP-PAA hydrogel (generated by Gemini AI tool). The hydrogel network incorporates GO sheets (hexagonal plates) and AgNPs (grey spheres) within a poly(acrylic acid) matrix. The composite hydrogel exhibits dual antimicrobial mechanisms: (i) direct antibacterial action through nanoparticle-bacteria interactions, and (ii) reactive oxygen species (ROS) generation leading to bacterial membrane disruption. Together, these mechanisms enable switchable swelling, antimicrobial activity, and potential applications in smart wound healing and regenerative medicine.

2.7. Cytotoxicity assay

Biocompatibility of the hydrogels was assessed using Vero (African green monkey kidney epithelial), HeLa (human cervical carcinoma), and BHK-21 (baby hamster kidney fibroblast) cell lines. Cell lines and the necessary culture media were obtained from the Centre for Advanced Research in Sciences, University of Dhaka, where the cytotoxicity assays were carried out. Cells were cultured in Dulbecco's Modified Eagle's Medium (DMEM) supplemented with 10% fetal bovine serum (FBS), 1% penicillin-streptomycin, and 0.2% gentamycin. Cells were seeded in 96-well plates at densities of 1.5×10^4/100 μL (Vero and BHK-21) and 2.0×10^4/100 μL (HeLa), and incubated at 37 °C with 5% CO_2. After 24 h, autoclaved hydrogel samples were added to the wells. Cytotoxicity was investigated using an inverted light microscope after 48 h of incubation, and cell morphology and viability were compared with untreated controls. All experiments were performed in duplicate.

The inclusion of cytotoxicity studies was vital to confirm the safety of the hydrogels for biomedical use. A non-toxic profile against mammalian cells is essential for any wound healing application, ensuring that while the hydrogel prevents bacterial growth, it does not damage surrounding tissues. Fig. 2 illustrates the dual antimicrobial mechanism, where the hydrogel inhibits bacterial growth through both direct AgNP/GO interaction and ROS-mediated membrane disruption.

3. Results and discussion

3.1. Mechanistic approach for the formation of GO-AgNP-PAA hydrogels

The formation of hydrogels using silver nitrate, GO and acrylic acid monomer in the presence of a thermal initiator is presented in Fig. 3. It is evident that in the presence of $K_2S_2O_8$, the system forms radicals that promote hydrogen evolution. First, $AgNO_3$ dissociates into Ag^+, which is reduced and deposited on graphene oxide (GO) to form an Ag/GO catalyst. Acrylic acid polymerizes on GO, forming a PAA-GO hybrid rich in –COOH groups. $K_2S_2O_8$ decomposes to produce sulfate radicals ($SO_4^{\bullet -}$), which react with water to generate $^{\bullet}OH$ and H^+. These protons are reduced on Ag nanoparticles with electron transfer through GO, producing hydrogen gas: $2H^+ + 2e^- \rightarrow H_2$. Furthermore, $K_2S_2O_8$ acts as a radical initiator for acrylic acid polymerization. These radicals attack the double bond of acrylic acid, initiating chain growth and forming poly(acrylic acid) on the GO surface, improving stability and catalytic activity.

3.2. Confirmation of GO formation and interfacial interactions in GO-AgNP-PAA

ATR-IR spectroscopy verified the successful synthesis of GO and its integration within the poly(acrylic acid) (PAA) network. The GO spectrum (Fig. 4a) displayed the expected bands: a broad –

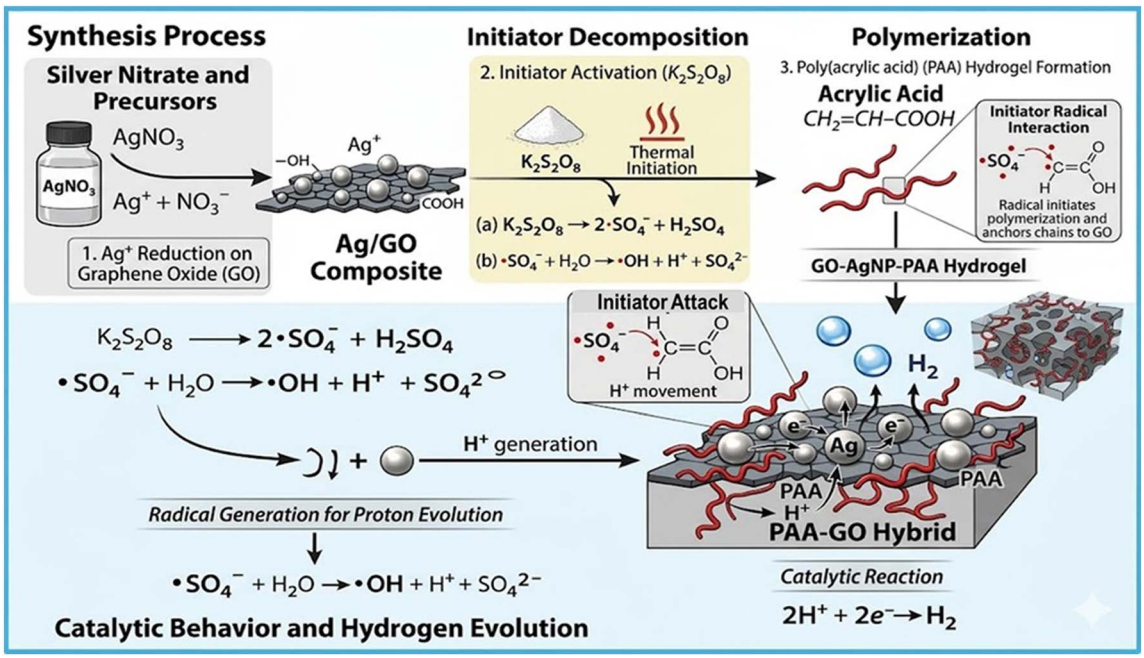

Fig. 3 Schematic of the reaction mechanism involved in the formation of GO-AgNP-PAA hydrogel (generated by Gemini AI tool).

OH stretch at ~3380 cm^{-1}, carboxyl C=O at ~1721 cm^{-1}, and C–O (alkoxy/epoxy) features near ~1030 cm^{-1}, consistent with the oxidation of graphite to GO.[41–43] Additional bands at ~2980 cm^{-1} (aliphatic C–H) and ~1372 cm^{-1} (C–OH bend) corroborate the presence of oxygenated groups, while the ~1628 cm^{-1} H–O–H bend indicates adsorbed water, typical for hydrophilic GO sheets; a weak O=C=O feature around ~2351 cm^{-1} is sometimes observed in stored films.

Upon incorporation into the hydrogel, the GO-AgNP-PAA spectrum shows a broadened –OH envelope (~3438 cm^{-1}), attributable to hydrogen bonding among PAA chains, interstitial water, and GO oxygenated groups.[44] The prominent band at ~1701 cm^{-1} (PAA C=O stretch) increases in intensity relative to AgNP-PAA, indicating additional carbonyl content and/or strengthened hydrogen-bonding microenvironments introduced by GO. The presence of aliphatic C–H (~2933 and 2556 cm^{-1}), $-CH_2$ deformation (~1394 cm^{-1}), and C–O/C–O–C bands (~1180 and ~1004 cm^{-1}) confirms polymer formation and ester/ether linkages within the network.[41,45] Compared to AgNP-PAA, the spectral changes in GO-AgNP-PAA (band broadening and modest shifts) suggest specific interfacial interactions (H-bonding and van der Waals) between PAA and GO that can modulate network hydration and swelling—features central to the observed switchable behavior.

Robust hydrogen bonding and hydrophilicity at the filler-polymer interface support high water content, conformability, and pH-responsive swelling, all of which are desirable for exudate management and comfort in wound dressings. An ATR-IR spectroscopic study analyzed the functional groups on GO (Fig. 4a). The characteristic peaks are shown in the figure, which indicate the successful synthesis of GO. In the ATR-IR spectrum of GO, the peak at 3380 cm^{-1} is correlated to the –OH vibration stretching. The peaks at 1721 cm^{-1} and 1030 cm^{-1} correspond to carboxyl C=O stretching and alkoxy C–O stretching, respectively, situated at the edges of the GO nanosheets.[22] The peak at 2980 cm^{-1} corresponds to the aliphatic C–H bond and the peak at 1372 cm^{-1} corresponds to tertiary alcoholic C–OH bending. The peak at 1628 cm^{-1} corresponds to H–O–H water bending and the peak at 2351 cm^{-1} corresponds to the presence of O=C=O. The results are in accordance with published works on GO.[42,43] The curve marked as GO-AgNP-PAA proves good dispersion of GO in the PAA matrix and the successful fabrication of the GO-AgNP-PAA hydrogel. The hydrogen bonds and van der Waals forces between the PAA and GO make the absorption band of the –OH groups wider with the addition of GO.[45] Compared to AgNP-PAA, the GO-AgNP-PAA curve has increased absorption at 1701 cm^{-1}, indicating the successful addition of GO to the PAA matrix.

The ATR-IR spectrum of the GO-AgNP-PAA gel displayed peaks at 3438 cm^{-1} for the –OH vibrational stretching of water molecules as the reaction was carried out in aqueous solution. The peaks at 2933 cm^{-1} and 2556 cm^{-1} correspond to the aliphatic C–H bonds. The broad absorption band at 1701 cm^{-1} indicates the carboxylic acid group (C=O) vibrational stretching of PAA. The peak at 1394 cm^{-1} is related to the $-CH_2$ group. The peaks at 1180 cm^{-1} and 1004 cm^{-1} are related to ester groups (C–O–C) and C–O stretching respectively.[41,45]

3.3. Scanning electron microscope analysis

The SEM image of GO (Fig. 5a) shows a randomly aggregated, thin and crumpled layer structure. The van der Waals attraction causes the wrinkled GO nanosheets to ripple and entangle with each other. The lateral dimensions of these transparent nanosheets are in the nanometer-to-micrometer range. These morphological characteristics are very similar to those previously reported.[46,47]

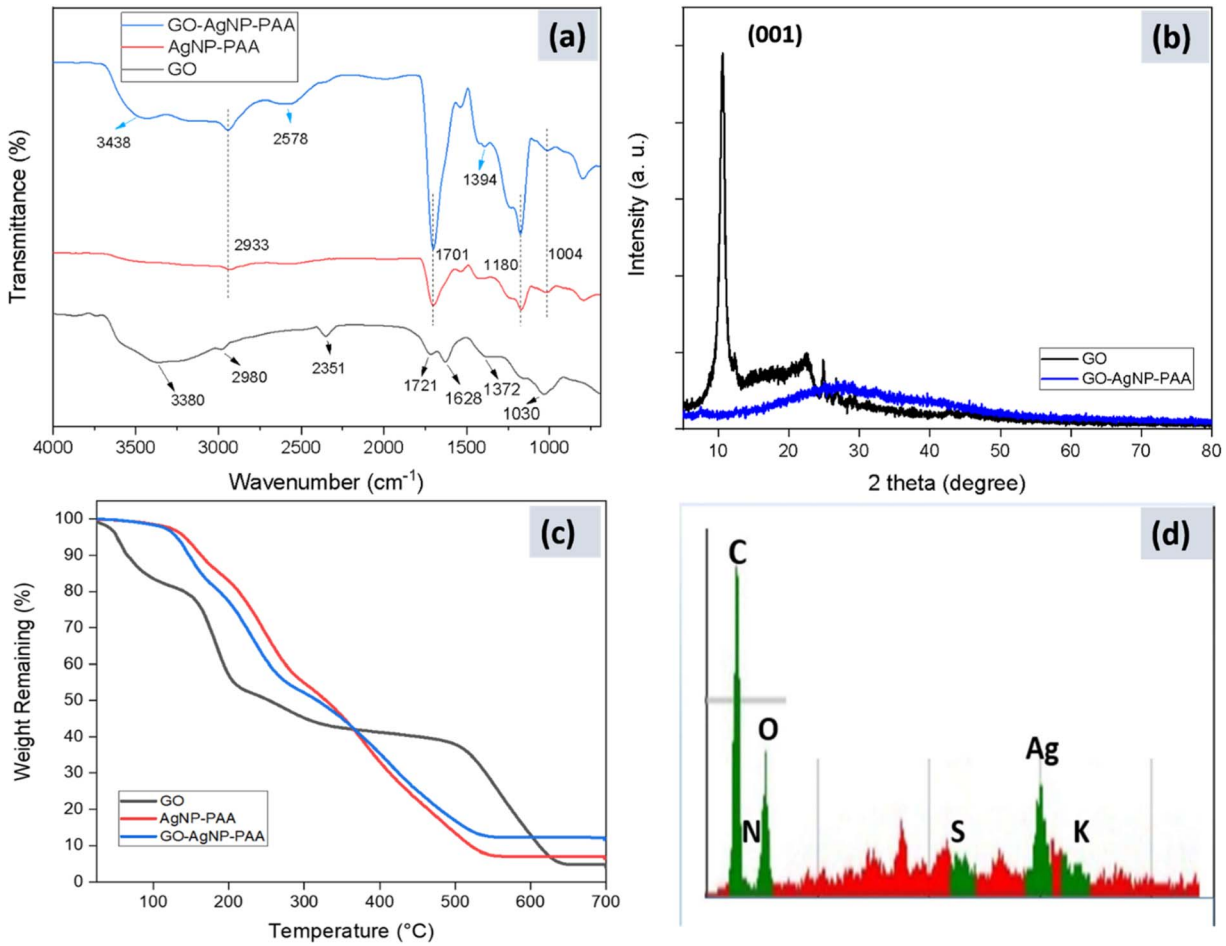

Fig. 4 Comprehensive characterization of synthesized materials. (a) ATR-IR spectra of GO, the AgNP-PAA hydrogel, and the GO-AgNP-PAA hydrogel showing the presence of oxygen-containing functional groups (–OH, C=O, and C–O) and confirming the successful incorporation of GO and AgNPs within the PAA matrix. (b) XRD patterns of GO and the GO-AgNP-PAA hydrogel, where the disappearance of the sharp GO peak at 10.56° and broad scattering between 20–40° indicate the uniform dispersion of GO in the polymeric network and *in situ* formation of AgNPs. (c) TGA thermograms of GO, the AgNP-PAA hydrogel, and the GO-AgNP-PAA hydrogel demonstrating the enhanced thermal stability of the composite hydrogel due to strong interfacial interactions between GO sheets, AgNPs, and the PAA network. (d) EDS spectrum of the GO-AgNP-PAA hydrogel, confirming the elemental composition (C, O, Ag, *etc.*) and supporting the structural integration of GO and AgNPs in the hydrogel matrix.

Fig. 5b and c shows the SEM images of hydrogels before and after the addition of GO. Significant differences were observed in the morphology of the hydrogel after GO was added to the polymer matrix. The addition of GO imparts a rough, spongy surface morphology that can enhance its adsorption properties. It also confirms the successful addition of GO into the PAA hydrogel.

Fig. 5d and e shows the FESEM images of the GO-AgNP-PAA hydrogel. FESEM images of the hydrogel reveal that the as-formed AgNPs were homogeneously and uniformly deposited on the surface of the GO nanosheets to obtain a gel-based nanocomposite system. A little variation in the surface morphology of the GO-AgNP-PAA hydrogel is due to the electrostatic and π–π interactions and hydrogen bonding between GO, AgNP and PAA due to the presence of carboxyl, epoxy and hydroxyl groups.[48] At 500 00× magnification, the nanoparticles could be seen; 100 particles were arbitrarily selected from the image, their diameters were measured with respect to the scale of 100 nm, and the average size of the particles was calculated to be *ca.* 13 nm (Fig. 5f).

3.4. X-ray diffraction pattern analysis

XRD studies of the as-prepared GO and the GO-AgNP-PAA hydrogel were carried out to confirm the successful synthesis of GO and its uniform distribution in the PAA matrix. Fig. 4b shows the XRD pattern of the GO flakes and the GO-AgNP-PAA hydrogel. The peak at 10.56° confirms the formation of GO nanosheets. This diffraction peak corresponds to the (001) plane of GO with a *d*-spacing of 0.846 nm, which is much larger than pristine graphite because of the addition of oxygen functional groups after chemical oxidation and exfoliation.[49–51]

The broad scattering at 2θ values between 20° and 40° indicates the relatively amorphous nature of the GO-AgNP-PAA hydrogel. The synthesized GO-AgNP-PAA hydrogel shows no characteristic peak of GO at 10.56°, indicating the uniform

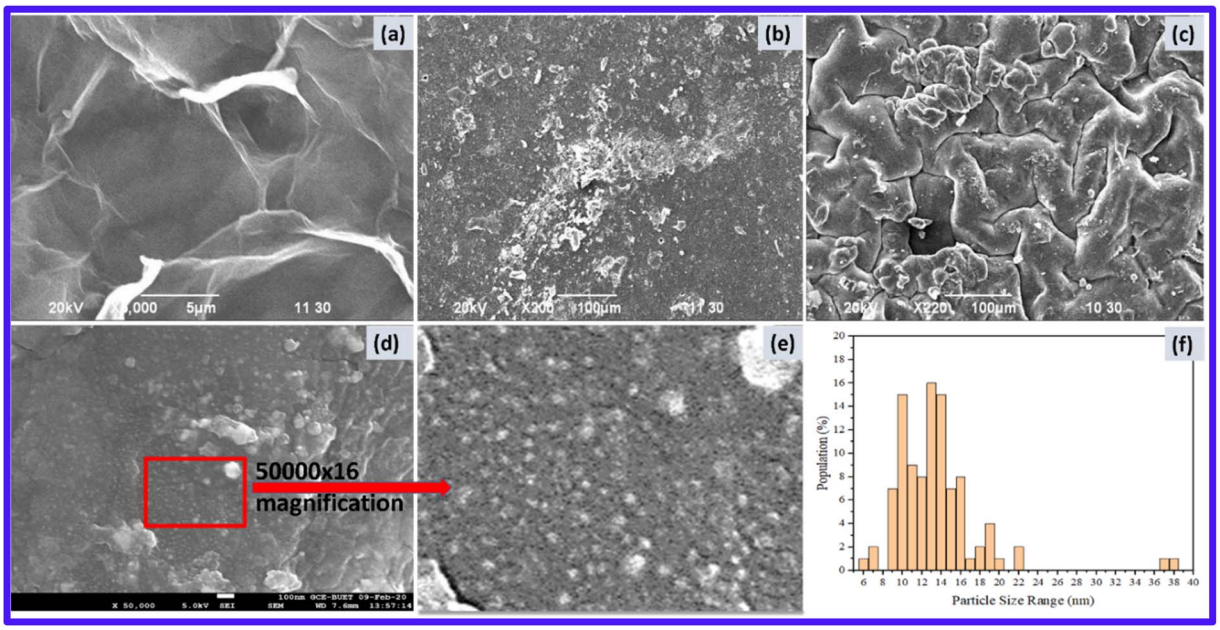

Fig. 5 Morphological analysis of graphene oxide (GO), AgNP-PAA hydrogel, and GO-AgNP-PAA hydrogel. (a) SEM image of GO showing the wrinkled, crumpled, and layered sheet-like morphology typical of exfoliated nanosheets. (b) SEM image of the AgNP-PAA hydrogel displaying relatively smooth polymeric surfaces in the absence of GO. (c) SEM image of the GO-AgNP-PAA hydrogel, revealing a rough, porous, and sponge-like structure after GO incorporation, confirming the successful dispersion in the hydrogel matrix. (d and e) FESEM images of GO-AgNP-PAA hydrogel at different magnifications showing uniform distribution of in situ-synthesized AgNPs on GO nanosheets and within the polymeric network. (f) Particle size distribution of AgNPs embedded in the hydrogel, with an average size of ~13 nm, validates the nanoscale uniformity, crucial for antimicrobial performance.

distribution of GO into the polymer matrix without any ordered aggregation.[42]

The EDS spectrum of the GO-AgNP-PAA hydrogel is shown in Fig. 4d. The elemental composition of the GO-AgNP-PAA hydrogel is derived from the spectrum. The EDS spectrum of the prepared hydrogel shows the presence of carbon, nitrogen, oxygen, silver, potassium and sulfur, in agreement with the results obtained from ATR-IR, XRD, and SEM, *etc.*

3.5. Thermogravimetric analysis

TGA was done to investigate the thermal stability of the hydrogel and to compare its behavior before and after the addition of graphene oxide. Fig. 4c shows the TGA curves of graphene oxide, the AgNP-PAA hydrogel and the GO-AgNP-PAA hydrogel.

From Fig. 4c, it can be seen that GO was less thermally stable compared to the hydrogels. For GO, around 20% weight loss occurred due to the temperature increase from room

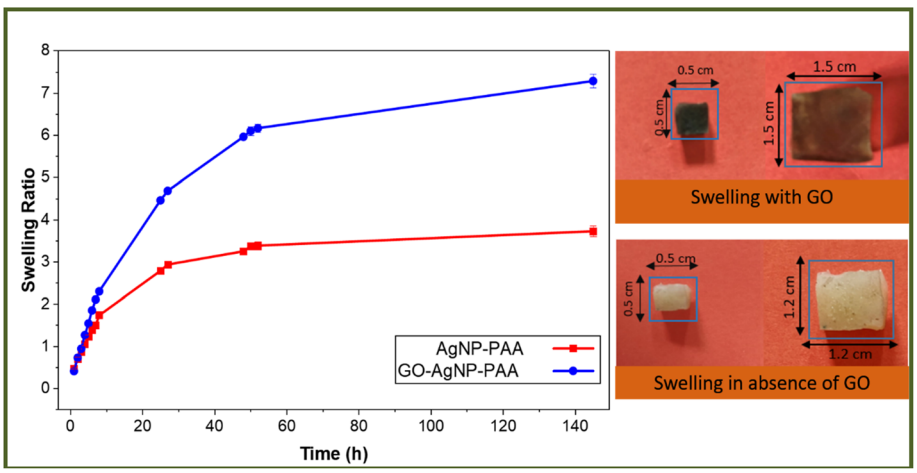

Fig. 6 Comparative swelling behavior of AgNP-PAA and GO-AgNP-PAA hydrogels in distilled water ($n = 3$, mean ± SD). The differences in equilibrium swelling ratios is statistically significant ($p < 0.05$).

temperature to 150 °C, from the loss of bound water. Around 55% of its weight loss occurred below 200 °C because functional groups having labile oxygen decompose at this temperature.[52,53] In the temperature range of 200–500 °C, the weight loss remains somewhat constant, which can be attributed to the conversion of GO to graphene. Above this temperature, again, a rapid weight loss occurs up to 640 °C due to the diminishing structure of graphene under extremely high temperatures. The constant weight after this temperature up to 700 °C is due to the remaining residues of salts, acids, *etc.*

It can also be seen that the incorporation of GO into the polymer increased the thermal stability above 360 °C, suggesting a strong interaction between the polymer and GO.[42] The weight loss of the polymer occurs in a regular manner from 120 °C to 550 °C, not following the weight reduction pattern of GO, suggesting that GO is well dispersed and an integral component of the hydrogel. The curve shows the degradation in this range due to the breakdown of linear carbon-carbon chains and crosslinked polymer networks[54,55]

3.6. Swelling behavior of the GO-AgNP-PAA hydrogel

To investigate the swelling behavior of the GO-AgNP-PAA hydrogel and to observe the effects of GO incorporation, two hydrogels, one containing both the AgNP and GO, and another containing only AgNP, were dried and immersed in distilled water until a constant weight was obtained. The hydrogels were removed from the water at regular intervals, blotted with filter paper and weighed. The swelling ratio was calculated using the following equation:

$$\text{Swelling ratio} = \frac{W_s - W_d}{W_d}$$

where W_s and W_d are the mass of swollen and dried hydrogels, respectively.

All swelling experiments were performed in triplicate, and the results are presented as mean ± standard deviation. Statistical significance between samples was evaluated using a two-tailed Student's *t*-test.

Fig. 6 shows that the incorporation of GO into the hydrogel dramatically increased the swelling property of the hydrogel. Both the hydrogels reached equilibrium at about 2 hours. The swelling ratio of 7.29 of the hydrogel containing GO at equilibrium was more than double (an increase of almost 204%) that of the hydrogel not containing GO, which showed a swelling ratio of 3.58.

The role of GO sheets is crucial because after the addition of GO, the hydrogel showed drastically enhanced swelling properties without distortion of the gel structure. The unique structure of GO sheets might impart some hydrophilic character when they are homogeneously dispersed in the gel network. The GO sheets have a large number of hydrophilic groups like –COOH, –C═O, –OH and –C–O–C⁻on their surfaces, which improve the interfacial interactive favorable microenvironment for channeling solvent molecules, and the rigidity of the thin sheet cut the continuous hydrogen bonding within intra-/inter-polymer attraction, which seems to be responsible for enhancing the swelling capacity of the prepared hydrogel.[24] A synergistic intermolecular interaction between GO sheets and the PAA polymer matrix might also be a reason for the increased water holding capacity of the hydrogel.

3.7. On–off switching of GO-AgNP-PAA hydrogel

The swelling behavior of the AgNP-PAA and GO-AgNP-PAA hydrogels was studied in distilled water. Distilled water is generally considered neutral, but a slightly acidic pH of around 6.8 was used for this experiment. A mechanistic depiction of the swelling and collapsed states of the hydrogel is presented in Fig. 7a. pH-regulation in antagonistic, harsh environments reversibly affects the swelling behavior of the hydrogels. Therefore, we used 0.1 M NaOH and 0.1 M HCl as two separate aqueous solutions to investigate the on–off (expanded-collapsed) switching of only the GO-AgNP-PAA hydrogel. At first, a piece (500 mg) of the as-prepared hydrogel was immersed in 0.1 M NaOH solution for 12 h, and an equilibrium state of hydrated hydrogel was obtained. Free water was wiped from the hydrated gel, followed by weighing and immersion of the gel into 50 mL of 0.1 M HCl.

In alkaline environments, the hydrogel network expands due to the ionization of carboxyl groups on poly(acrylic acid), generating electrostatic repulsion and enhanced solvent uptake (ON state). Conversely, in acidic environments, protonation of carboxyl groups reduces charge repulsion, leading to network

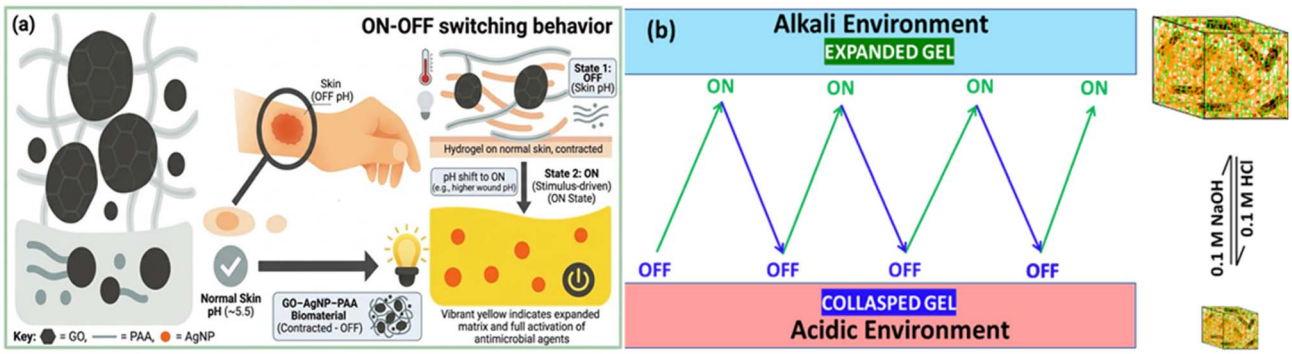

Fig. 7 pH-controlled on–off switching behavior of the GO-AgNP-PAA hydrogel: (a) mechanistic view and (b) different experimental cycles (partly generated by the Gemini AI tool).

Table 1 Diameters of the zones of inhibition (ZOI) for different bacteria, obtained using AgNP-PAA and GO-AgNP-PAA hydrogels. Data are expressed as mean, $n = 3$

Sample name	Concentration (mg mL^{-1})	*E. coli* (mm)	*P. aeruginosa* (mm)	*K. pneumonia* (mm)	*S. aureus* (mm)
Ag-PAA gel	10 (S1)	0	6	9	0
	20 (S2)	0	7	13	7
	30 (S3)	0	10	17	11
Ag-GO-PAA gel	10 (C1)	0	0	0	0
	20 (C2)	11	9	5	8
	30 (C3)	18	15	10	14

collapse and shrinkage (OFF state) as shown in Fig. 7b. The cyclic swelling–deswelling transition demonstrates the reversible responsiveness of the hydrogel to external pH stimuli, a key property for programmable drug delivery, smart wound healing, and tissue engineering applications.[56]

3.8. Antibacterial activity study

The *in vitro* antibacterial screening of the GO-AgNP-PAA hydrogel and AgNP-PAA hydrogel was investigated against both Gram-positive and Gram-negative bacterial strains and the results are presented in Table 1. The antibacterial activity was measured based on the diameter of the inhibition zone. The surrounding clear zone was considered as an inhibitory zone and the contact area was used to evaluate growth inhibition underneath (Fig. 8).

In all cases, increasing the concentration of the hydrogel increases the inhibition zone. For the Gram-positive *Staphylococcus aureus* (*S. aureus*) bacteria, the highest antibacterial activity was achieved at a concentration of 30 mg mL^{-1} for both hydrogels. Although the AgNP-PAA hydrogel shows antimicrobial activity in the absence of graphene oxide, the activity is enhanced from 11 mm to 14 mm when graphene oxide is present. The enhanced antibacterial activity in the presence of GO may be associated with interference in the YycFG two-component transduction system, as reported in previous studies. As a result, the signaling system through which the bacterial strains adapt to environmental stresses is damaged and the bacterial viability, cell membrane metabolism regulation, and cell wall synthesis are hampered[57,58] Further molecular-level studies are required to directly confirm the involvement of the YycFG signaling pathway in GO-mediated antibacterial activity.

The antimicrobial activity of the AgNP-PAA and GO-AgNP-PAA hydrogels was tested against three different strains of Gram-negative bacteria, *Klebsiella pneumonia* (*K. pneumonia*) ATCC,

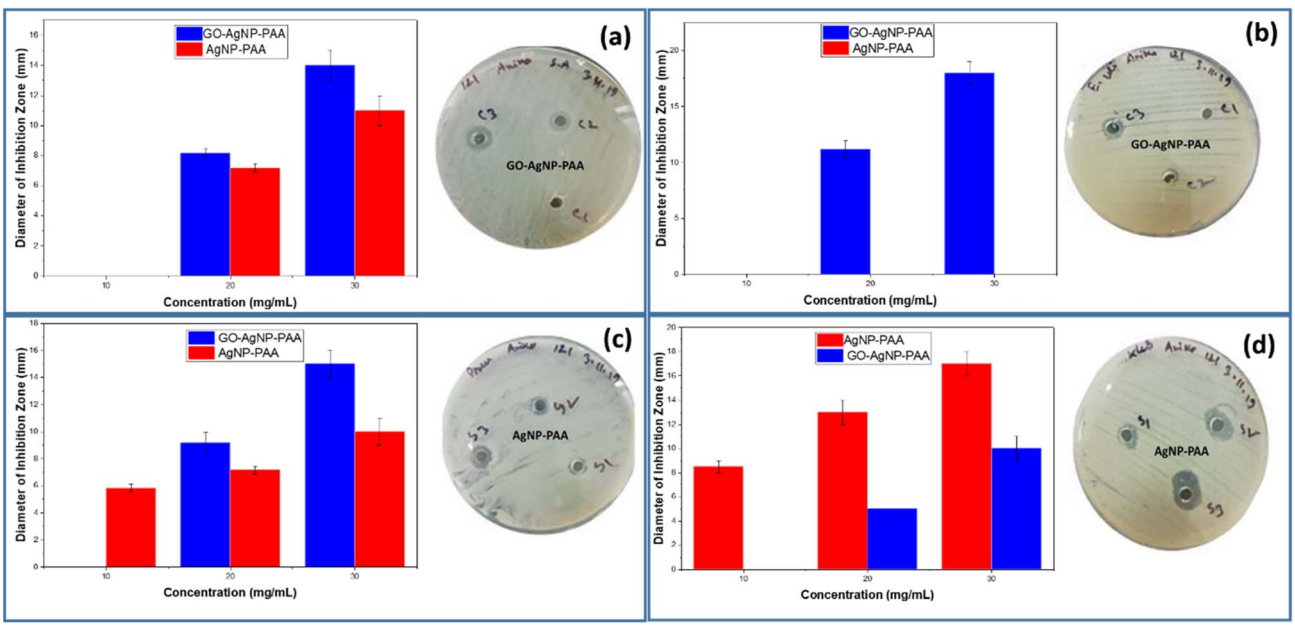

Fig. 8 Comparative antibacterial activity of AgNP-PAA and GO-AgNP-PAA hydrogels against different bacterial strains at varying concentrations. The diameter of the zone of inhibition (ZOI) was measured for (a) *Staphylococcus aureus* (b) *Escherichia coli*, (c) *Klebsiella pneumoniae*, and (d) *Pseudomonas aeruginosa*. (Error bars represent standard deviation (SD), $n = 3$.) The plots show a concentration-dependent increase in antibacterial efficacy, with GO-AgNP-PAA hydrogels exhibiting larger inhibition zones than AgNP-PAA in most cases, demonstrating synergistic enhancement due to graphene oxide's high surface area and improved Ag^+ ion release. A slight reduction in activity against *P. aeruginosa* suggests strain-specific differences in resistance. The inset photographs depict representative agar plates showing inhibition zones around the hydrogel samples.

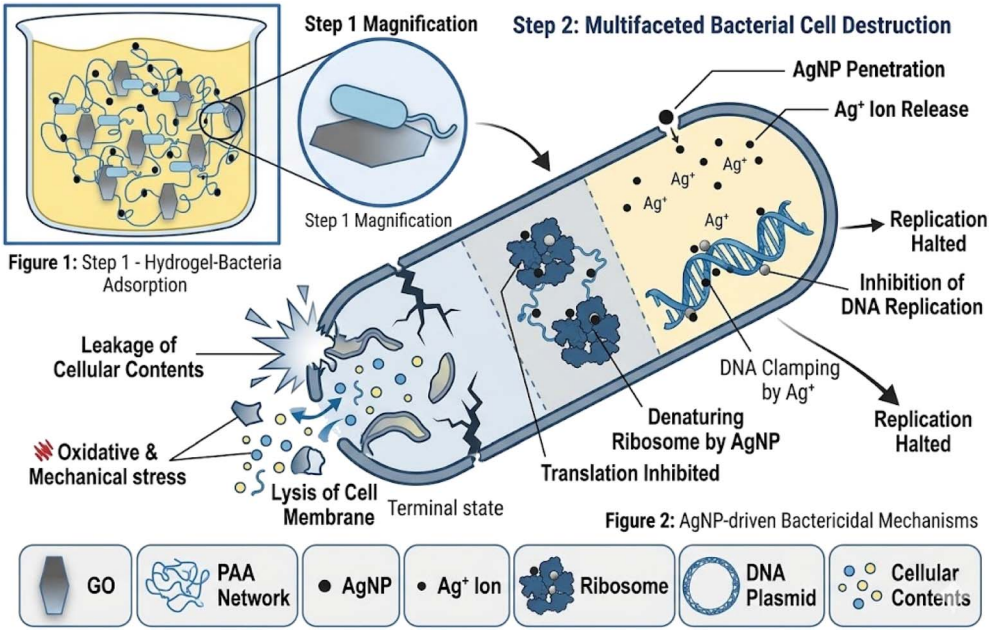

Fig. 9 Proposed mechanism of the antibacterial activity of the GO-AgNP-PAA hydrogel (generated by the Gemini AI tool). The schematic illustrates the two-step antibacterial mechanism. Step 1: Bacteria adsorb onto the graphene oxide (GO) surface of the hydrogel through electrostatic interactions and physical trapping. Step 2: The incorporated silver nanoparticles (AgNPs) penetrate the bacterial cell wall, causing membrane disruption and leakage of cellular contents. Released Ag^+ ions interact with intracellular components, leading to ribosome denaturation, inhibition of DNA replication, and eventual bacterial cell death. The synergistic effect of GO and AgNPs enhances antibacterial efficiency by combining mechanical membrane damage with strong oxidative and ionic stress.

Escherichia coli (*E. coli*) ATCC, and *Pseudomonas aeruginosa* (*P. aeruginosa*) ATCC. For the Gram-negative *P. aeruginosa*, both hydrogels show high antimicrobial activity at 30 mg mL^{-1}. The antimicrobial activity was clearly enhanced in the presence of GO after 10 mg ml^{-1}. At 30 mg mL^{-1}, the largest diameter was achieved for GO-AgNP-PAA at 15 mm compared to 10 mm for AgNP-PAA. The effect of the addition of GO on increasing the antimicrobial activity of the hydrogels is most evident in the case of the Gram-negative *E. coli*. The AgNP-PAA gel showed no antimicrobial activity, whereas the GO-AgNP-PAA showed significant activity. The highest inhibition zone of 18 mm was achieved at 30 mg mL^{-1} for GO-AgNP-PAA. This is the highest inhibition zone observed for all the bacterial strains tested. Without GO, there was no observable antimicrobial activity against *E. coli.* The exfoliation and sharp blade-like edges in GO increase the interlayer distance and solubility, which causes more effective disruption of the bacterial cell wall.[59] The presence of GO also increases the nanomaterial-bacteria interfacial contact area, which significantly increases the antibacterial activity.[60]

The activity against the Gram-negative bacteria *Klebsiella* was different from the previous observations. Here, higher activity was observed in the absence of GO. Both hydrogels showed antimicrobial activity, with the largest inhibition zone being 17 mm for AgNP-PAA compared to 10 mm for GO-AgNP-PAA. The antibacterial activity largely depends on several parameters, such as the GO and AgNP percentage in the hydrogel. There must be an optimum concentration of GO and AgNPs for a particular bacterial strain. After reaching a specific peak activity against bacteria, further increase in the percentage of GO and AgNPs might lower the activity.[60,61] The addition of GO might reduce the bactericidal activity by consuming the active sites of PAA and further research should be initiated to optimize the amount of GO in the composite hydrogel.

3.9. Mechanism of antibacterial activity

In the age of drug resistance, antimicrobial polymers can be a powerful tool to fight against bacterial and fungal infections. It is evident from the diameters of the inhibition zones that in the presence of GO, the highest antimicrobial activity was observed for the AgNP-PAA hydrogel at a concentration of 30 mg mL^{-1}, which was found to be active against both Gram-positive and Gram-negative bacterial strains (except for *Klebsiella pneumonia*, which showed higher activity in the absence of GO). This behavior can be attributed to the synergistic bactericidal effect of both GO and AgNPs.

Antibacterial activity is largely dependent on size and the bactericidal effect increases with decreasing size. The small-

Table 2 Cytotoxicity of AgNP-PAA and the GO-AgNP-PAA hydrogel on the Vero, HeLa and BHK-21 cell lines

	Survival of cells (%)		
Sample type	Vero	HeLa	BHK-21
Solvent−	100	100	100
Solvent+	>95	>95	>95
Ag NPs-PAA hydrogel	>95	>95	>95
GO-Ag NPs-PAA hydrogel	>95	>95	>95

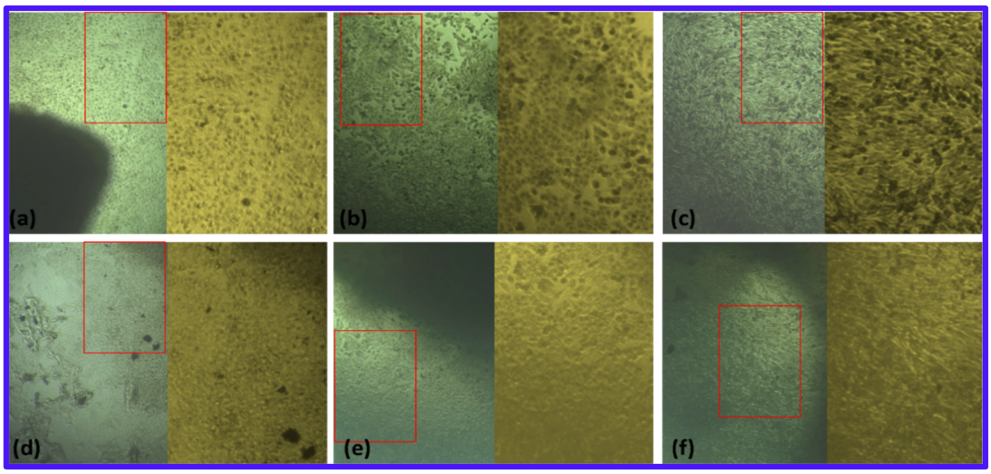

Fig. 10 Inverted light microscope images showing the cytocompatibility of AgNP-PAA and GO-AgNP-PAA hydrogels with different cell lines. Panels (a–c) represent Vero, HeLa, and BHK-21 cells cultured with the AgNP-PAA hydrogel, while panels (d–f) show the corresponding cell lines treated with the GO-AgNP-PAA hydrogel. The GO-AgNP-PAA hydrogel exhibits improved cell attachment, spreading, and growth compared to AgNP-PAA, indicating enhanced biocompatibility due to the synergistic interaction of graphene oxide with the polymer matrix, which supports a better cell-material interface and reduced cytotoxicity.

sized AgNPs pass through the cell membrane and bacterial replication is hampered. The AgNPs present in the hydrogel matrix diffuse out, accumulate, form aggregates, and show a strong interaction with the lipid layer of the cell membrane.[62] At this stage, the bacterial membrane integrity diminution and perforation occur, which lead to cellular death.[63] High oxidative stress, caused by the reactive oxygen species (ROS) generated from the AgNPs, is also considered a primary mode of cytotoxic action that causes cellular inactivation.[64,65] Moreover, AgNPs denature the ribosomes, which inhibits protein synthesis, leading to plasmic membrane degradation (Fig. 9). They can also bind with the DNA, thus hindering the DNA replication and ultimately inhibiting bacterial reproduction. The high adsorption capacity of GO and negatively charged polymers help the bacterial cell to adsorb on the hydrogel surface. Thus, the increased contact between bacteria and the nanocomposite hydrogel causes a synergistic effect.[66]

3.10. The cytotoxicity effect of the hydrogels

The cytotoxicity of the synthesized AgNP-PAA and GO-AgNP-PAA hydrogels was evaluated using three mammalian cell lines, namely, Vero, HeLa, and BHK-21, to determine their biocompatibility. As summarized in Table 2, both hydrogels exhibited excellent cell viability, with survival rates exceeding 95% for all tested cell lines, indicating negligible cytotoxicity. The solvent control maintained 100% viability, confirming the absence of any interference or inherent toxicity from the culture medium.

The inverted light microscope images (Fig. 10) further support these findings. Cells exposed to the AgNP-PAA hydrogel (Fig. 10a–c) maintained normal morphology and attachment, whereas those treated with the GO-AgNP-PAA hydrogel (Fig. 10d–f) displayed enhanced proliferation, spreading, and confluence. This observation suggests improved cytocompatibility and cell-material interactions due to the synergistic influence of graphene oxide within the composite matrix.

The superior performance of the GO-AgNP-PAA hydrogel can be attributed to the unique properties of graphene oxide (GO), which offer a high surface area, oxygen-containing functional groups, and enhanced hydrophilicity, thereby facilitating protein adsorption and cell adhesion. The incorporation of GO also contributes to better mechanical strength, surface roughness, and wettability, promoting a more favorable microenvironment for cellular growth. Meanwhile, the PAA polymer network provides a soft and hydrated structure that mimics the natural extracellular matrix, further supporting cell attachment and viability. The combination of AgNPs with GO and PAA thus results in a hydrogel system that is both antibacterial and biocompatible, striking a balance between antimicrobial efficacy and cellular safety. The cytotoxicity results clearly indicate that these hydrogels are suitable for interaction with living tissues without inducing toxic effects.

Overall, the study has demonstrated that both AgNP-PAA and GO-AgNP-PAA hydrogels exhibit excellent cytocompatibility, with the GO-containing formulation showing slightly superior biological performance. These findings confirm that the developed hydrogels hold great promise for diverse biological and environmental applications, including wound healing, biosensing, antibacterial coatings, and water purification.[67–69]

4. Conclusion

The simple, easy and fast synthesis of the GO-based, Ag nanoparticle-incorporated poly (acrylic acid) hydrogel has been demonstrated, without the use of any environmentally hazardous solvent or cross-linker. The GO-AgNP-PAA hydrogel was characterized using suitable characterization tools that confirmed the successful synthesis of the nanoparticles and the incorporation of GO into the polymer matrix. The size of the nanoparticles from FESEM images was found to be in the range of 10–20 nm. It was found that the swelling of the hydrogel

increased by almost 204% after the addition of GO. GO also increased the thermal stability and antimicrobial activity of the hydrogel. The synthesized nanocomposite hydrogel showed enhanced antibacterial activity against both Gram–positive and Gram-negative bacterial strains. This hydrogel showed no cytotoxic effect on Vero, HeLa, and BHK-21 cell lines. The antimicrobial activity of the hydrogel, combined with the absence of its cytotoxic effect, makes it an excellent candidate for further study of its application in the biomedical field.

Author contributions

Anika Tabassum Promi: investigation; Md. Kaium Hossain: writing – original draft and data analysis; Shaikat Chandra Dey, Aanshi Tiwari, Nusrat Mustary: methodology writing – review and editing, and visualization; Md. Mizanur Rahaman, Otun Saha, Ayushi Tiwari, Yogesh Shukla: visualization, validation, writing – review and editing; Ashutosh Tiwari: conceptualization, validation, writing – review and editing; and Md. Ashaduzzaman: supervision, funding acquisition, writing – review and editing. The manuscript was written with contributions from all authors. All authors have read and agreed to the published version of the manuscript.

Conflicts of interest

The authors declare that there is no conflict of interest related of this article.

Data availability

All data generated or analysed during this study are included in this published article.

Acknowledgements

The authors are thankful to the Ministry of Science and Technology, Government of the People's Republic of Bangladesh (Project number: EAS–437/1773) and International Association of Advanced Materials, Sweden, for providing financial support to carry out this research. Md. Ashaduzzaman extends his heartfelt thanks to the International Association of Advanced Materials, Sweden, for their cooperation and exchange of knowledge to construct the research work. He also thanks the Centre for Advanced Research and Sciences, University of Dhaka, Bangladesh, for the instrumental support.

References

1 A. S. Hoffman, *Adv. Drug Deliv. Rev.*, 2012, **64**, 18–23.
2 E. Caló and V. V. Khutoryanskiy, *Eur. Polym. J.*, 2015, **65**, 252–267.
3 Y. Sharma, A. Tiwari, S. Hattori, D. Terada, A. K. Sharma, M. Ramalingam and H. Kobayashi, *Int. J. Biol. Macromol.*, 2012, **51**, 627–631.
4 H. K. Patra, Y. Sharma, M. M. Islam, M. J. Jafari, N. A. Murugan, H. Kobayashi, A. P. F. Turner and A. Tiwari, *Nanoscale*, 2016, **8**, 17213–17222.
5 O. Wichterle and D. Lím, *Nature*, 1960, **185**, 117–118.
6 E. M. Ahmed, *J. Adv. Res.*, 2015, **6**, 105–121.
7 J. Li and D. J. Mooney, *Nat. Rev. Mater.*, 2016, **1**, 16071.
8 N. A. Peppas, J. Z. Hilt, A. Khademhosseini and R. Langer, *Adv. Mater.*, 2006, **18**, 1345–1360.
9 A. Mishra, T. Omoyeni, P. K. Singh, S. Anandakumar and A. Tiwari, *Int. J. Biol. Macromol.*, 2024, **276**, 133823.
10 A. M. Lever and R. N. Borazjani, *Contact Lens Anterior Eye*, 2001, **24**, 94–99.
11 D. G. Ahearn, D. T. Grace, M. J. Jennings, R. N. Borazjani, K. J. Boles, L. J. Rose, R. B. Simmons and E. N. Ahanotu, *Curr. Microbiol.*, 2000, **41**, 120–125.
12 A. Dixit, A. Sabnis and A. Shetty, *J. Mater. Process. Technol.*, 2022, **8**, 2699–2715.
13 J. S. Boateng, K. H. Matthews, H. N. E. Stevens and G. M. Eccleston, *J. Pharm. Sci.*, 2008, **97**, 2892–2923.
14 S. Dhivya, V. V. Padma and E. Santhini, *Biomedicine*, 2015, **5**, 22.
15 E. A. Kamoun, E.-R. S. Kenawy and X. Chen, *J. Adv. Res.*, 2017, **8**, 217–233.
16 M. C. Koetting, J. T. Peters, S. D. Steichen and N. A. Peppas, *Mater. Sci. Eng. R Rep.*, 2015, **93**, 1–49.
17 S. Schreml, R.-M. Szeimies, L. Prantl, M. Landthaler and P. Babilas, *J. Am. Acad. Dermatol.*, 2010, **63**, 866–881.
18 H. H. Leveen, G. Falk, B. Borek, C. Diaz, Y. Lynfield, B. J. Wynkoop, C. A. Mabunda, I. L. Rubricius and G. C. Christoudias, *Ann. Surg.*, 1973, **178**, 745–753.
19 R. Barbucci, in. *Hydrogels: Biological Properties and Applications*, Springer Milan, Milano, 2009.
20 A. V. Kabanov and S. V. Vinogradov, *Angew. Chem., Int. Ed.*, 2009, **48**, 5418–5429.
21 N. A. Peppas and E. W. Merrill, *J. Appl. Polym. Sci.*, 1977, **21**, 1763–1770.
22 Y. Feng, B. Chen, M. Zhang, R. Cheng, X. Su and Y. Feng, *Mater. Des.*, 2025, **256**, 114309.
23 K. Haraguchi, *Curr. Opin. Solid State Mater. Sci.*, 2007, **11**, 47–54.
24 D. R. Dreyer, S. Park, C. W. Bielawski and R. S. Ruoff, *Chem. Soc. Rev.*, 2010, **39**, 228–240.
25 S. Sharma, M. Bhende, P. Mulwani, V. Patil, H. R. Verma and S. Kumar, *Int. J. Biol. Macromol.*, 2025, **289**, 139481.
26 O. Akhavan and E. Ghaderi, *ACS Nano*, 2010, **4**, 5731–5736.
27 S. Liu, T. H. Zeng, M. Hofmann, E. Burcombe, J. Wei, R. Jiang, J. Kong and Y. Chen, *ACS Nano*, 2011, **5**, 6971–6980.
28 L. Zhang, J. Xia, Q. Zhao, L. Liu and Z. Zhang, *Small*, 2010, **6**, 537–544.
29 S. Lee, H. Lee, J. H. Sim and D. Sohn, *Macromol. Res.*, 2014, **22**, 165–172.
30 M. Rai, A. Yadav and A. Gade, *Biotechnol. Adv.*, 2009, **27**, 76–83.
31 J. R. Morones, J. L. Elechiguerra, A. Camacho, K. Holt, J. B. Kouri, J. T. Ramírez and M. J. Yacaman, *Nanotechnology*, 2005, **16**, 2346–2353.

32 T. C. Dakal, A. Kumar, R. S. Majumdar and V. Yadav, *Front. Microbiol.*, 2016, **7**, 1831.
33 P. Rujitanaroj, N. Pimpha and P. Supaphol, *Polymer*, 2008, **49**, 4723–4732.
34 H. Haidari, R. Bright, X. L. Strudwick, S. Garg, K. Vasilev, A. J. Cowin and Z. Kopecki, *Acta Biomater.*, 2021, **128**, 420–434.
35 A. C. M. D. Moraes, B. Araujo Lima, A. Fonseca De Faria, M. Brocchi and O. Luiz Alves, *Int. J. Nanomed.*, 2015, **10**(1), 6847–6861.
36 A. M. Aboulella, A. Alabi, M. R. A. Shehhi and L. Zou, *Water Environ. Res.*, 2025, **97**, e70110.
37 S. L. Percival, S. M. McCarty and B. Lipsky, *Adv. Wound Care*, 2015, **4**, 373–381.
38 J. Dissemond, M. Witthoff, T. C. Brauns, D. Haberer and M. Goos, *Hautarzt*, 2003, **54**, 959–965.
39 A. Panáček, M. Smékalová, R. Večeřová, K. Bogdanová, M. Röderová, M. Kolář, M. Kilianová, Š. Hradilová, J. P. Froning, M. Havrdová, R. Prucek, R. Zbořil and L. Kvítek, *Colloids Surf. B Biointerfaces*, 2016, **142**, 392–399.
40 A. W. Bauer, W. M. M. Kirby, J. C. Sherris and M. Turck, *Am. J. Clin. Pathol.*, 1966, **45**, 493–496.
41 A. Boukir, S. Fellak and P. Doumenq, *Heliyon*, 2019, **5**, e02477.
42 H. Zhang, D. Zhai and Y. He, *RSC Adv.*, 2014, **4**, 44600–44609.
43 H.-P. Cong, P. Wang and S.-H. Yu, *Chem. Mater.*, 2013, **25**, 3357–3362.
44 Z. Tai, J. Yang, Y. Qi, X. Yan and Q. Xue, *RSC Adv.*, 2013, **3**, 12751.
45 I. Zojaji, A. Esfandiarian and J. Taheri-Shakib, *Adv. Colloid Interface Sci.*, 2021, **289**, 102314.
46 H. Saleem, M. Haneef and H. Y. Abbasi, *Mater. Chem. Phys.*, 2018, **204**, 1–7.
47 T. Yeh, J. Syu, C. Cheng, T. Chang and H. Teng, *Adv. Funct. Mater.*, 2010, **20**, 2255–2262.
48 H. K. Ismail, L. I. A. Ali, H. F. Alesary, B. K. Nile and S. Barton, *J. Polym. Res.*, 2022, **29**, 159.
49 M. Muniyalakshmi, K. Sethuraman and D. Silambarasan, *Mater. Today Proc.*, 2020, **21**, 408–410.
50 X. Sun, Z. Liu, K. Welsher, J. T. Robinson, A. Goodwin, S. Zaric and H. Dai, *Nano Res.*, 2008, **1**, 203–212.
51 D. S. R. Josephine, B. Sakthivel, K. Sethuraman and A. Dhakshinamoorthy, *ChemistrySelect*, 2016, **1**, 2332–2340.
52 Y. Xu, K. Sheng, C. Li and G. Shi, *ACS Nano*, 2010, **4**, 4324–4330.
53 J. Liu, G. Chen and M. Jiang, *Macromolecules*, 2011, **44**, 7682–7691.
54 S. S. A. Kumar, N. B. Manik, K. M. Batoo, I. A. Wonnie Ma, K. Ramesh, S. Ramesh and M. A. Shah, *Sci. Rep.*, 2023, **13**, 8946.
55 W. Li, P. Luo and X. Wang, *Polymers*, 2025, **17**, 1999.
56 A. Tiwari, J. J. Grailer, S. Pilla, D. A. Steeber and S. Gong, *Acta Biomater.*, 2009, **5**, 3441–3452.
57 S. Wu, J. Zhang, Q. Peng, Y. Liu, L. Lei and H. Zhang, *Antibiotics*, 2021, **10**, 1555.
58 S. Wu, T. Gan, L. Xie, S. Deng, Y. Liu, H. Zhang, X. Hu and L. Lei, *Biomater. Adv.*, 2022, **141**, 213121.
59 K. Chaturvedi, K. Yadav, A. Singhwane, R. Chowdhary, R. K. Mohapatra, A. K. Srivastava and S. Verma, *BioNanoScience*, 2025, **15**, 189.
60 C. Hu, Y. Yang, Y. Lin, L. Wang, R. Ma, Y. Zhang, X. Feng, J. Wu, L. Chen and L. Shao, *Adv. Drug Deliv. Rev.*, 2021, **178**, 113967.
61 X. Li, J. Sun, Y. Che, Y. Lv and F. Liu, *Int. J. Biol. Macromol.*, 2019, **121**, 760–773.
62 R. Sahraei and M. Ghaemy, *Carbohydr. Polym.*, 2017, **157**, 823–833.
63 B. Le Ouay and F. Stellacci, *Nano Today*, 2015, **10**, 339–354.
64 P. V. AshaRani, G. Low Kah Mun, M. P. Hande and S. Valiyaveettil, *ACS Nano*, 2009, **3**, 279–290.
65 S. Kim and D.-Y. Ryu, *J. Appl. Toxicol.*, 2013, **33**, 78–89.
66 W.-P. Xu, L.-C. Zhang, J.-P. Li, Y. Lu, H.-H. Li, Y.-N. Ma, W.-D. Wang and S.-H. Yu, *J. Mater. Chem.*, 2011, **21**, 4593.
67 A. M. Salama, Z. Alqarni, Y. S. Hamed, K. Yang, H. F. Nour and J. Lu, *J. Drug Deliv. Sci. Technol.*, 2024, **95**, 105630.
68 Md. K. Hossain, A. Mishra, A. Tiwari, B. Pant, S. C. Dey, A. Tiwari, O. Saha, Md. M. Rahaman, Y. R. Shukla, A. Tiwari and Md. Ashaduzzaman, *SN Appl. Sci.*, 2023, **5**, 339.
69 S. Durairaj, D. Sridhar, G. Ströhle, H. Li and A. Chen, *ACS Appl. Mater. Interfaces*, 2024, **16**, 18300–18310.